

# Efflorescence assessment using hyperspectral imaging for concrete structures

Byunghyun Kim<sup>a</sup> and Soojin Cho<sup>\*</sup>

Department of Civil Engineering, University of Seoul,  
163 Seoulsiripdae-ro, Dondaemun-gu, Seoul 02504, Republic of Korea

(Received May 20, 2017, Revised November 18, 2017, Accepted November 28, 2017)

**Abstract.** Efflorescence is a phenomenon primarily caused by a carbonation process in concrete structures. Efflorescence can cause concrete degradation in the long term; therefore, it must be accurately assessed by proper inspection. Currently, the assessment is performed on the basis of visual inspection or image-based inspection, which may result in the subjective assessment by the inspectors. In this paper, a novel approach is proposed for the objective and quantitative assessment of concrete efflorescence using hyperspectral imaging (HSI). HSI acquires the full electromagnetic spectrum of light reflected from a material, which enables the identification of materials in the image on the basis of spectrum. Spectral angle mapper (SAM) that calculates the similarity of a test spectrum in the hyperspectral image to a reference spectrum is used to assess efflorescence, and the reference spectral profiles of efflorescence are obtained from the USGS spectral library. Field tests were carried out in a real building and a bridge. For each experiment, efflorescence assessed by the proposed approach was compared with that assessed by image-based approach mimicking conventional visual inspection. Performance measures such as accuracy, precision, and recall were calculated to check the performance of the proposed approach. Performance-related issues are discussed for further enhancement of the proposed approach.

**Keywords:** hyperspectral imaging; efflorescence; concrete; spectral angle mapper

## 1. Introduction

Efflorescence is one of the important phenomena that cause concrete degradation including cracks, spalling, delamination, segregation, and rebar exposure. Although efflorescence does not severely harm structural safety in the short term, it may result in severe damage to structural integrity in the long term. Although efflorescence develops on the concrete surface, the concrete loses its alkalinity, which may cause corrosion of the rebar inside. Thus, efflorescence should not be overlooked as a simple aesthetic problem, and must be accurately assessed with proper inspection. For example, efflorescence is a rating indicator of concrete structures in the guideline for the structural safety inspection in Korea (MOLIT 2016).

Currently, efflorescence is assessed mostly on the basis of visual inspection executed by professional inspectors. In the current visual inspection, efflorescence is determined on the basis of its white color, and the criteria depend strongly on the unquantified expertise and subjective decision of the inspectors. Many studies have been reported on replacing visual inspection with objective computer vision-based detection for various types of concrete defects (Adhikari *et al.* 2014, Liu *et al.* 2014, Man *et al.* 2015, Dawood *et al.*

2017), while there are few on the efflorescence detection. In the field of efflorescence management, it is recommended that efflorescence be measured by considering the lightness (closely related to intensity) of images in the CIELab color system (BASF 2014 and Cemex USA 2008). A photo-spectrometer is recommended for stable measurement under varying environmental conditions, whose pointwise measurement may not be applicable for large structures. González-Jorge *et al.* (2013) used the light intensity profile from LiDAR data to detect the efflorescence on a masonry arch structure; detection was based on the subjective decision of a threshold that is changeable according to the inspectors' expertise. Image-based inspection can speed the assessment of large structures, whereas quantitative and objective efflorescence assessment is still not allowed because light intensity is the sole parameter to assess efflorescence.

Hyperspectral imaging (HSI) is an emerging technique that allows identification of materials in an image on the basis of the electromagnetic spectrum of the reflected light (Chang 2003, Grahn and Geladi 2007). HSI has been widely used in agriculture (Jun *et al.* 2016), environment (Zhang *et al.* 2016), surveillance (Proto *et al.* 2010), biomedical imaging (Regeling *et al.* 2016), geosciences (Udelhoven *et al.* 2017), and mineralogy (van der Werff 2006). For example, ElMasry *et al.* (2012) measured the freshness of beef using HSI as an integrated alternative to a traditional colorimeter, standard pH electrodes, and universal testing machines for measuring the color, pH, and tenderness of beef, respectively. Caughlin *et al.* (2016) measured growth rates of 20 species of tropical trees using

---

\*Corresponding author, Assistant Professor

E-mail: soojin@uos.ac.kr

<sup>a</sup> Graduate Student

E-mail: shdik2002@uos.ac.kr

HSI to predict landscape variation and found that the visible and near-infrared regions are relatively important for relating canopy reflectance to tree growth data. The examples show that HSI can be a good alternative to visual inspection as well as image-based inspection without losing either accuracy or scalability.

Despite its capability, implementation of HSI in the civil engineering area is found to be quite limited. Vaghefi *et al.* (2011) implemented various image-based techniques, including HSI, to the maintenance of bridges in the US, and they evaluated HSI as a practical tool for detecting chemical leaching of concrete structure. Lee *et al.* (2012) carried out experimental research to develop a quantitative measurement technique for concrete strength using HSI-based remote sensing, with promising results was quite promising. Baseley *et al.* (2016) detected dimethyl methyl phosphonate, which is a surrogate for common organophosphate pesticides, from building walls using HSI. Santos *et al.* (2017) found the crack distribution against biological colonization around the cracks using HSI and k-means clustering. However, the application of HSI to objective efflorescence detection has never been reported at the best knowledge of the present authors.

In this paper, a novel approach is proposed for the objective and quantitative assessment of concrete efflorescence using HSI. The proposed approach provides a 2D distribution map of efflorescence on the concrete surface based on a spectral angle mapper (SAM) (Kruse *et al.* 1993) representing the similarity of the spectral profiles as a form of angle. The HSI device used in this research acquires spectral profiles of reflected light over the visible and near infrared (VNIR) region between 300 nm and 1000 nm with spectral resolution of 1.31 nm. The reference spectral profiles of efflorescence and normal concrete was first obtained from USGS Spectral Library Version 7 (Kokaly *et al.* 2017), and the similarity is calculated using SAM at each pixel of the hyperspectral image. The similarity threshold to find the corresponding material was determined on the basis of experimental results. Validation of the proposed approach was carried out on a real building and a bridge. For each experiment, the efflorescence obtained by the proposed approach was compared with those obtained by a lightness-based approach mimicking conventional visual inspection. The results were numerically illustrated using performance measures including accuracy, precision, and recall.

## 2. Efflorescence assessment using hyperspectral imaging

### 2.1 Hyperspectral imaging

An HSI device collects and processes information from across the light spectrum. HSI acquires the light spectrum from each pixel in the image of a scene and identifies materials in the pixels using their unique spectral characteristics. In HSI, the collected light spectra cover a wide range of wavelengths with fine wavelength resolution. The features of the light spectra, such as slope, absorption,

local peak and reflectance are taken from the hyperspectral images and processed to identify the materials and/or their conditions in the pixels (Heiden *et al.* 2007). The implementations have reported strong performance in the identification of materials using the spectral characteristics and their features, especially in the identification of visually similar materials that are difficult to distinguish with common vision systems (i.e., camera).

### 2.2 Spectral angle mapper

SAM is a spectral classification tool that permits rapid mapping of the similarity of two spectra as a form of an “angle” (Kruse *et al.* 1993). SAM treats spectra as vectors in a space with dimensionality equal to the number of bands ( $nb$ ). SAM assumes that a single pixel or certain group of pixels in HSI represents one certain material, and the same material can be found by comparing the similarity between spectra. The angle ( $\alpha$ ) between a test spectrum and reference spectrum can be derived from the arc-cosine of the dot product of two spectra defined as a geometric vector as

$$\alpha = \cos^{-1} \left( \frac{\mathbf{t} \cdot \mathbf{r}}{\|\mathbf{t}\| \cdot \|\mathbf{r}\|} \right) = \cos^{-1} \left( \frac{\sum_{i=1}^{nb} t_i r_i}{\left( \sum_{i=1}^{nb} t_i^2 \right)^{1/2} \left( \sum_{i=1}^{nb} r_i^2 \right)^{1/2}} \right) \quad (1)$$

### 2.3 Spectral characteristics of efflorescence and concrete

To identify efflorescence on a concrete surface, the main chemical components of efflorescence and concrete must be investigated *a priori*, because spectrum characteristics are highly dependent on the chemical components within a material. First, concrete is a composite material composed of aggregate and cementitious material. Generally, the concrete surface is covered by mortar paste, whose main components are calcium silicate hydrate and calcium hydroxide, which are produced during the hydration process (Taylor and Harry 1997).

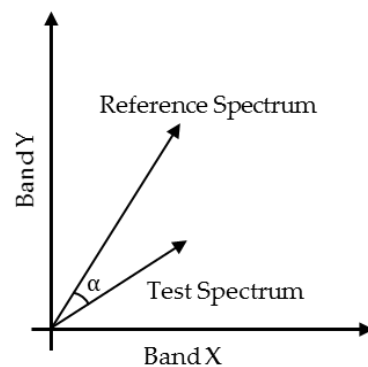


Fig. 1 Simplified SAM example with two bands (Redrawn from Kruse *et al.* (1993))

Meanwhile, efflorescence is a crystalline deposit, usually bright-colored, that forms on or near the surface of concrete products. Efflorescence usually consists of calcium carbonate ( $\text{CaCO}_3$ ), a product material of soluble materials such as calcium hydroxide ( $\text{Ca}(\text{OH})_2$ ) and carbon dioxide ( $\text{CO}_2$ ) in the atmosphere, as illustrated in Fig. 2. To analyze efflorescence by detecting calcium carbonates on a concrete surface, the spectra of calcium carbonate and concrete were first obtained from the United States Geological Survey (USGS) spectral library (USGS Spectral Library 2017). The USGS spectral library offers full spectrum plots of major components of various earth minerals. The USGS library does not contain a profile for calcium carbonate but does for calcite, which is a carbonate mineral and the most stable polymorph of calcium carbonate (Anthony *et al.* 2003). Among the five available spectra of calcite in the USGS library, two spectra (Calcite CO2004 and Calcite HS48.3B) were selected because of their spectral purity. In addition, a spectrum of concrete (Concrete WTC01-37A) was found in the USGS library. Though the USGS library provides full profiles in the range of 200–3000 nm, only the spectra in the range of 400–1000 nm were investigated because the HSI imaging device used in this study captures spectrum in the 400–1000 nm range only.

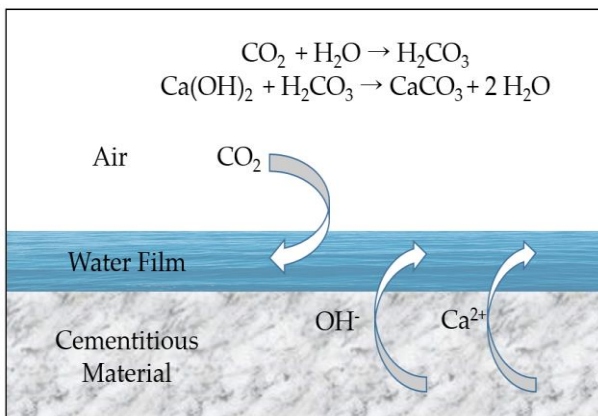


Fig. 2  $\text{CaCO}_3$  formation on cementitious material

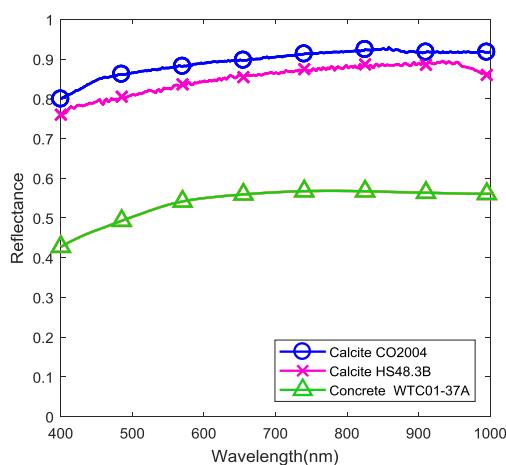


Fig. 3 Spectra of calcite and concrete in the USGS spectral library in the 200–1000 nm range

Fig. 3 shows the spectra of two calcites and a concrete in the 400–1000 nm range. The spectra of pure calcites shown in Fig. 3 have a high reflectance rate of approximately 80–90% and show a gentle slope in the visible and near-infrared (VNIR) spectrum range. At the same time, the spectrum of concrete shown in Fig. 3 has a relatively low reflectance rate of approximately 50% and shows a relatively steep spectrum difference near 550–600 nm. This infers that the efflorescence and concrete can be distinguished by the shape of their spectra.

#### 2.4 Proposed approach for efflorescence assessment using HSI

Because the shape of the efflorescence spectrum differs from that of the concrete spectrum, a SAM that quantifies the spectrum similarity is proposed for assessing efflorescence against concrete in an objective manner. Fig. 4 depicts a flowchart of the proposed approach to assess efflorescence using HSI. In the first step, the HSI device acquires the hyperspectral image of efflorescence on the surface of the concrete structure to be assessed. In the second step, the hyperspectral image is normalized using a barium sulfate reflector as a reflectance standard to remove the effect of lighting conditions. In this step, noisy bands due to inappropriate lighting conditions may be eliminated. In the third step, the spectral similarity of every pixel in the image is calculated using SAM by taking a reference spectrum of efflorescence. The reference spectrum of efflorescence is taken from the USGS spectral library in this study, but experimental spectrum may be used instead. In the fourth step, pixels with angles under a certain threshold are labeled as efflorescence, and they are mapped to visualize the shape of efflorescence. The threshold is determined as  $5^\circ$  for efflorescence in this study after a series of experiments, but the threshold may vary according to the chemical material to be assessed.

As an option, the area ratio of efflorescence can be obtained with pixels labeled as efflorescence. In Korea, the area ratio of efflorescence is requested for rating concrete structures by the guideline for safety inspection (MOLIT 2016). The area ratio is defined as the ratio of the efflorescence occurrence area to the unit inspection area. The efflorescence occurrence area is the area of a rectangle tightly bounding the efflorescence, and the unit inspection area is generally the structural element to be assessed, such as a span of a bridge girder or slab. According to the area ratio and the other inspection factors (e.g., cracking, leakage, and spalling), the inspected structure is graded from A to E, and its further maintenance is determined by the grade. Because real efflorescence generally has an unclear boundary, as discussed in the next section, the area ratio obviously depends on the subjective determination of efflorescence in the conventional visual inspection. Thus, the proposed approach based on HSI can provide objective assessment based on measurement results, not on the expertise of inspectors.

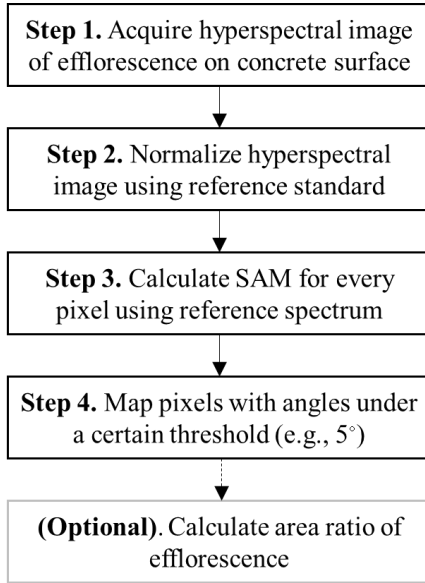


Fig. 4 Flowchart of efflorescence assessment using HSI

### 2.5 Evaluation of assessment result

The performance of the proposed approach was evaluated using three performance measures: accuracy, precision, and recall. The accuracy, precision, and recall can be written as

$$Accuracy = \frac{TP + TN}{TP + TN + FP + FN} \quad (2)$$

$$Precision = \frac{TP}{TP + FP} \quad (3)$$

$$Recall = \frac{TP}{TP + FN} \quad (4)$$

where  $TP$  is the true positive cases, where the approach predicts positive and the true answer is positive;  $TN$  is the true negative cases, where the approach predicts negative and the true result is negative;  $FP$  is the false positive cases, where the approach predicts positive but the true result is negative; and  $FN$  is the false negative cases, where the approach predicts negative but the true result is positive. In the efflorescence assessment, the positive means “labeled as efflorescence,” and negative means “labeled as concrete.” Thus, the accuracy means the number of pixels labeled correctly as efflorescence and concrete by the proposed approach among all pixels. The precision means the number of pixels labeled correctly as efflorescence by the proposed approach among all pixels labeled as efflorescence by the proposed approach. The recall means the number of pixels labeled correctly as efflorescence by the proposed approach among true efflorescence pixels.

## 3. Field experiments

To validate the performance of the proposed approach, field experiments were carried out on two concrete structures: a building at the University of Seoul and a concrete bridge pier. At the building, natural efflorescence was found near joints of the north and west walls of the first floor. At the concrete bridge pier, very thin natural efflorescence was observed, and an artificial efflorescence was drawn using a slate pencil made with natural limestone that is mostly composed of calcite. For our convenience, the four experiments were designated with abbreviations as tabulated in Table 1. The first letters, “W” and “P,” denote “Wall” and “Pier,” respectively, and the last letters “N” and “A” denote “Natural” and “Artificial” efflorescence, respectively.

### 3.1 Experimental setup

The experimental setup shown in Fig. 5 was shared for both field experiments. A hyperspectral camera along with a focusing lens (PS-VNIR, Specim, Spectral Imaging Ltd., Finland) was used in this study. The camera works as a push-broom type line-scan camera, and collects 2D images with the help of a rotary stage installed underneath. Its spectral range is 400–1000 nm in the visible and near infrared (VNIR) range, and it has 1392 (spatial)  $\times$  1040 (spectral) active pixels in full frame. The camera has a fore objective lens with focal length 23 mm. The camera is connected to a computer using a Firewire interface, and samples at 11 frames per second (fps) for full frame, and up to 62 fps when binning eight spectral bands together. The computer controls the camera using data acquisition software made by the manufacturer, and analyzes the acquired hyperspectral images using commercial software ENVI (Harris Corporation, FL, USA). For all experiments, the camera was located approximately 1.5 m distant from the test structure, and a 99% barium sulfate reflector was placed near the efflorescence for normalization. The reflector was installed near the test structure so as to share similar light conditions with the efflorescence.

### 3.2 Conventional RGB image-based approach

To evaluate the proposed approach, the conventional approach to assess efflorescence was carried out on RGB images rebuilt from the hyperspectral images. The RGB images were rebuilt by taking the spectral components according to red (690 nm), green (600 nm), and blue (520 nm) from the hyperspectral images, and thus the RGB images have the same sizes and pixel resolutions as the normalized hyperspectral images. The assessment of efflorescence from the RGB images was carried out using pixel intensity, and the thresholds were selected manually to mimic the visual inspection.

It notable that a single threshold was selected for each image “not to miss” possible efflorescence, because efflorescence is chemical leaching, and very thin efflorescence that is not harmful to the structure may occur on the concrete surface.

Table 1 Abbreviations of four field experiments.

Abbreviations	Details of Field Experiments
W1-N	Natural efflorescence on north side of a concrete wall of a building
W2-N	Natural efflorescence on west side of a concrete wall of a building
P1-N	Natural efflorescence on a pier of a bridge
P2-A	Artificial efflorescence made on a pier of a bridge

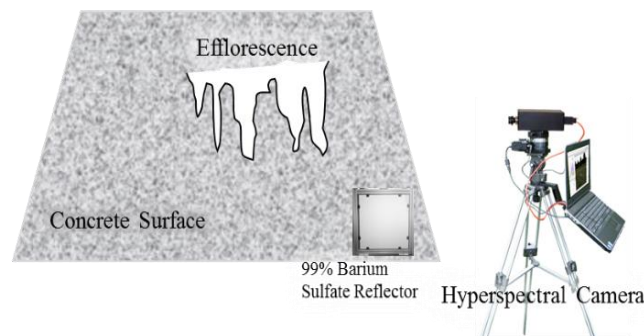


Fig. 5 Experimental setup



(a) Test Building



(b) Efflorescence on the north side of the concrete wall (W1-N)



(c) Efflorescence on the west side of the concrete wall (W2-N)

Fig. 6 Field experiment on a building

Thin efflorescence can also occur near the boundary of thick efflorescence. In this study, the threshold was conservatively selected to assess all white-colored efflorescence regardless of its thickness, which may result in overestimation in some cases.

### 3.3 Experiment on a building at the University of Seoul

The first field experiments (W1-N and W2-N) were conducted on a concrete wall of a building at the University of Seoul shown in Fig. 6(a). Efflorescence occurred at the north and west sides of the wall at the first floor of the building. The north side of the wall is approximately 10.5 m

wide and 3.85 m tall, and the west side is approximately 18 m wide and 3.65 m tall. Severe efflorescence was found at the joints on the wall as shown in Figs. 6(b) and 6(c), and two hyperspectral images were obtained around the efflorescence on both sides of the wall using the HSI setup in Fig. 5 during the daytime. Then, the proposed approach was applied to the obtained hyperspectral images. To calculate SAM, two reference spectra of calcite (Calcite CO2004 and Calcite HS48.3B) are taken from USGS spectral library version 7 (USGS Spectral Library 2017), and data from 420 nm to 850 nm, where the camera of this experiment can obtain data with a low spectral noise level, were used in the experiments.

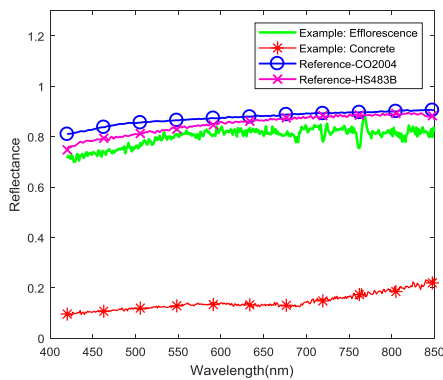


(a) RGB image rebuilt from the hyperspectral image

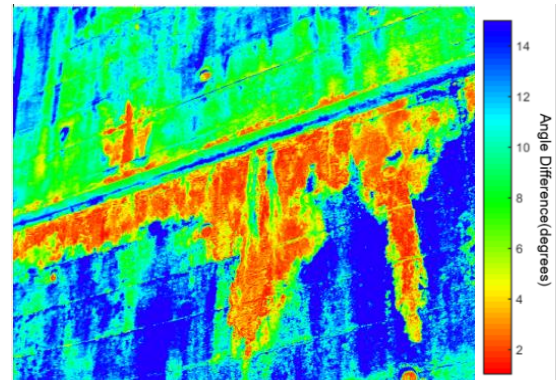


(b) Efflorescence assessment using intensity mimicking visual inspection

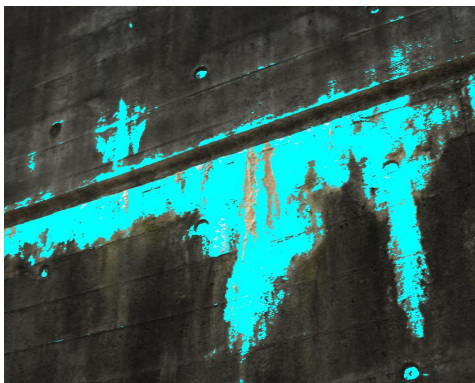
Fig. 7 Efflorescence assessment using an RGB image in case W1-N



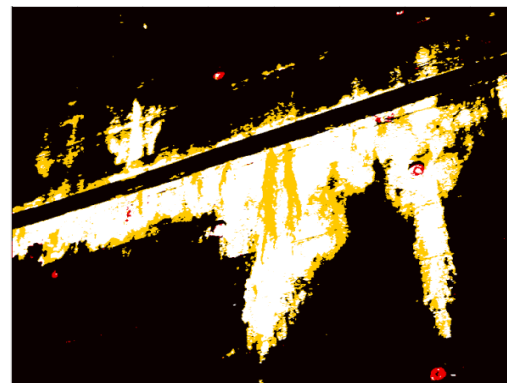
(a) Example spectra of efflorescence and concrete plotted with reference spectra



(b) Spectral angle (Reference: Calcite CO2004)



(c) Efflorescence assessment by the proposed approach using a 5° threshold



Legend: True positive (white), False positive (red), False Negative (yellow), True Negative (black)

(d) Distributions of TP, TN, FP, and FN referring to the assessment using the RGB image

Fig. 8 Efflorescence assessment by proposed approach for case W1-N

3.3.1 Assessment result for case W1-N

Fig. 7 shows the result of efflorescence assessment using the RGB image from W1-N. The image of W1-N has  $758 \times 692$  pixels, corresponding to 1.3 m wide and 0.8 m high around the efflorescence. For the RGB image shown in Fig. 7(a), 90 was selected as an intensity threshold to find

the efflorescence as shown in Fig. 7(b). As explained herein, the intensity threshold changes for every RGB image, because each RGB image has different intensity values of efflorescence and concrete, though they are rebuilt from the normalized hyperspectral image.

Fig. 8 shows the results of efflorescence assessment of W1-N by the proposed approach. Fig. 8(a) shows an example of spectra for efflorescence and concrete pixels picked up from the hyperspectral image of W1-N, compared to two reference spectra taken from the USGS library. In the range of 420–850 nm, the two reference spectra and the example spectrum of efflorescence are quite similar, whereas the example spectrum of concrete shows a clear disparity in the shape. Fig. 8(b) shows the spectral angle of the hyperspectral image obtained using SAM by taking the reference spectrum of Calcite CO2004. The pixels with angles of  $2^{\circ}$ – $4^{\circ}$  were colored with shades of red, those of  $5^{\circ}$ – $10^{\circ}$  were colored with shades of light green, and pixels with angles more than  $11^{\circ}$  were colored with shades of blue. Comparing Fig. 8(b) with Fig. 7(a) shows that the thick efflorescence corresponds to a small angle under  $5^{\circ}$ , whereas thin efflorescence has an angle between  $6^{\circ}$  and  $8^{\circ}$ . From the spectral angles, the pixels with angles smaller than  $5^{\circ}$  to the reference spectrum are overlapped on the RGB image in Fig. 8(c), which shows an overall shape of efflorescence similar to the result using the RGB image in Fig. 7(b). Then, the distributions of *TP*, *TN*, *FP*, and *FN* were visualized as shown in Fig. 8(d) by referring to the assessment using the RGB image. In Fig. 8(d), white and black pixels, respectively representing *TP* (i.e., correct labeling of efflorescence) and *TN* (i.e., correct labeling of concrete), are distributed along the overall shape of the efflorescence and concrete. Yellow pixels, representing *FN* (i.e., missing labeling of efflorescence), are distributed along the very thin efflorescence that is mostly on the boundary. Red pixels, representing *FP* (i.e., false labeling of efflorescence), are rarely detected. This result indicates the good performance of the proposed approach, although the very thin efflorescence and boundary are missing, as colored yellow.

### 3.3.2 Assessment result for case W2-N

The hyperspectral image from W2-N was processed similarly to that described in Section 3.3.1. The image of W2-N has  $647 \times 325$  pixels, corresponding to 0.4 m wide and 0.25 m high around the efflorescence. The result of efflorescence assessment using RGB image from W2-N was shown in Fig. 9. For the RGB image shown in Fig. 9(a), 140 was selected as an intensity threshold to find the efflorescence as shown in Fig. 9(b), which differs from 90 of W1-N. Fig. 10 shows the result of the efflorescence assessment of W2-N by the proposed approach. Similar to the result of W1-N, the thick efflorescence was detected appropriately using a  $5^{\circ}$  threshold, whereas thin efflorescence has an angle between  $6^{\circ}$  and  $8^{\circ}$  as shown in Fig. 10(a). The assessment result by the proposed method is shown in Fig. 10(b), which shows an overall good assessment. Fig. 10(c) shows the distributions of *TP*, *TN*, *FP*, and *FN* by referring to assessment using the RGB image in Fig. 9(b). Unlike the result of W1-N, W2-N has more pixels of *FN* and *FP*, and the reason is discussed in Section 4.

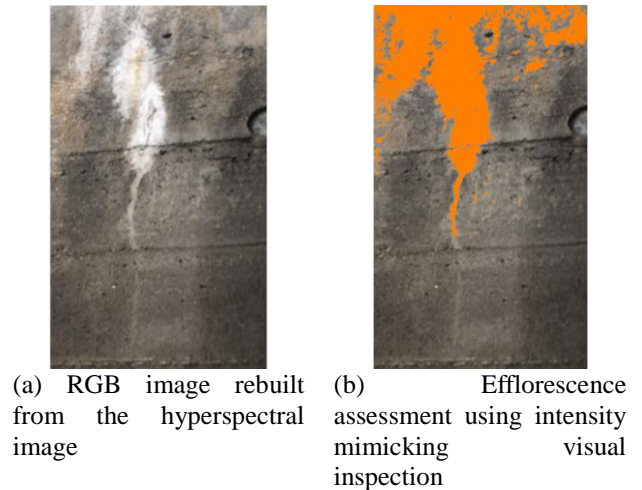


Fig. 9 Efflorescence assessment using RGB image in W2-N

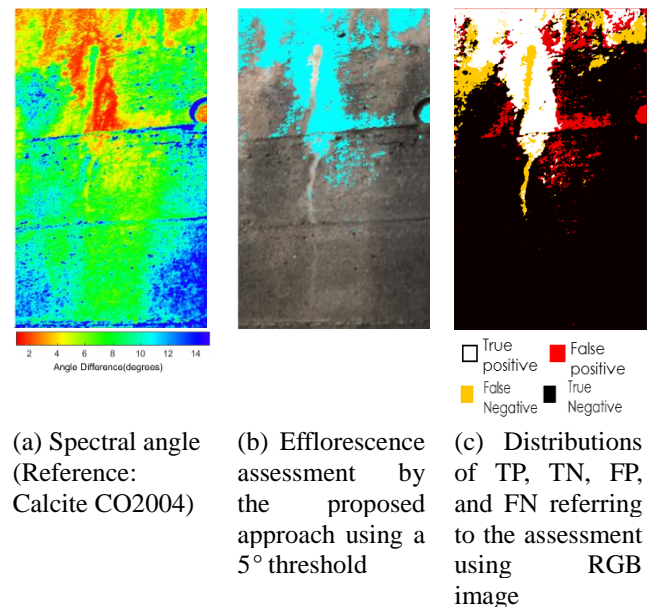


Fig. 10 Efflorescence assessment by proposed approach for W2-N

## 3.4 Experiment on a pier of a concrete bridge

Other field experiments (P1-N and P1-A) were conducted on a pier of a concrete bridge. The test bridge is a 20-span bridge with high concrete piers approximately 4 m wide and 20 m tall as shown in Fig. 11(a). Unlike the test building at the University of Seoul, the concrete of the bridge is light brown colored. Experiments on this brown color of the pier surface determined if the proposed approach using SAM is affected by the color of the concrete surface. On pier P19 of the bridge, a thin natural efflorescence was observed as flowing down along a micro crack of the concrete column as shown in Fig. 11(b). To increase the experimental case, an artificial efflorescence was drawn next to the natural efflorescence using a slate pencil made of a limestone. The artificial efflorescence was

drawn imitating the shape of the natural efflorescence as shown in Fig. 11(c). The hyperspectral camera was placed approximately 1.5 m distant from each target efflorescence, and the 99% barium sulfate reflector was located near the efflorescence.

3.4.1 Assessment result for case P1-N

Fig. 12 shows the result of efflorescence assessment using the RGB image from P1-N. The image of P1-N has  $303 \times 401$  pixels, corresponding to 0.5 m wide and 0.8 m high around the efflorescence. For the RGB image shown in Fig. 12(a), a high intensity threshold of 237 was selected because of the bright concrete color, and the efflorescence was obtained as Fig. 12(b). In this case, a considerable change in the obtained efflorescence was made by a small change in the intensity threshold, and Fig. 12(b) was obtained by many trial-and-error cycles to keep the shape of the efflorescence shown in Fig. 12(a). However, the obtained efflorescence has an unexpected irregular and discrete shape, which clearly shows a limitation of the intensity-based efflorescence assessment.

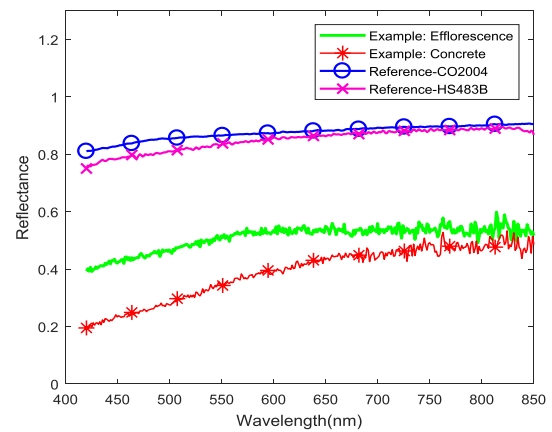
The proposed approach was applied to the hyperspectral image from P1-N as in Fig. 13. An example of spectra for efflorescence and concrete pixels is shown in Fig. 13(a), and the shapes of the spectra are different from those from the building in Fig. 8(a). The concrete has a spectrum with higher reflectance due to its bright color, and the efflorescence has a spectrum between the reference spectra and concrete spectrum because of its thinness. Fig. 13(b) is the mapped spectral angle, and Fig. 13(c) shows the assessed efflorescence using a  $5^\circ$  threshold.

the building in Fig. 8(a). The concrete has a spectrum with higher reflectance due to its bright color, and the efflorescence has a spectrum between the reference spectra and concrete spectrum because of its thinness. Fig. 13(b) is the mapped spectral angle, and Fig. 13(c) shows the assessed efflorescence using a  $5^\circ$  threshold.



(a) RGB image rebuilt from the hyperspectral image (b) Efflorescence assessment using intensity mimicking visual inspection

Fig. 12 Efflorescence assessment using RGB image in P1-N



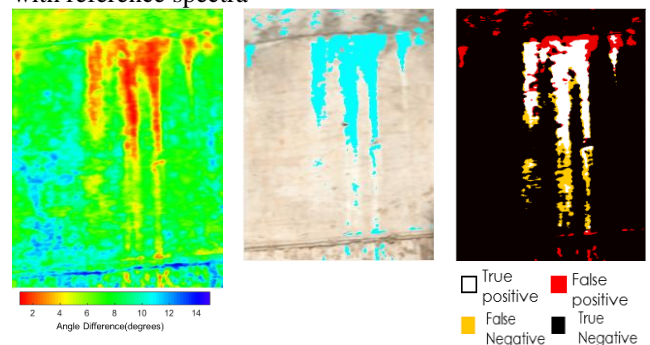
(a) Example spectra of efflorescence and concrete plotted with reference spectra



(a) Test Bridge



(b) Natural efflorescence on P19 (P1-N) (c) Artificial efflorescence on P19 (P2-A)



(b) Spectral angle (Reference: Calcite CO2004) (c) Efflorescence assessment by the proposed approach using a  $5^\circ$  threshold (d) Distributions of TP, TN, FP, and FN referring to assessment using RGB image

Fig. 13 Efflorescence assessment by proposed approach for P1-N

Fig. 11 Field experiment on a bridge

Unlike in the previous experiment, the  $5^\circ$  threshold provides good estimation with a smooth and regular shape compared to the result in Fig. 12(b). The distributions of  $TP$ ,  $TN$ ,  $FP$ , and  $FN$  in Fig. 13(d) shows many yellow and red pixels related to  $FN$  and  $FP$ , respectively. The yellow pixels are observed at the end of flows that are difficult to judge, and the red pixels are at the start of flow near the micro crack that is the source of the efflorescence. Considering the shape and the occurrence process of the efflorescence, it can be concluded that the proposed approach assessed the thin efflorescence better than the conventional method.

### 3.4.2 Assessment result for case P2-A

For the artificial efflorescence made with a slate pencil, the results by the conventional RGB-based and proposed approaches are briefly shown in Fig. 14. The image of P2-A has  $393 \times 534$  pixels, corresponding to 0.35 m wide and 0.65 m high around the efflorescence. For the RGB image shown in Fig. 14(a), 190 was selected as the intensity threshold, and the efflorescence was reasonably obtained as Fig. 14(b). Fig. 14(c) shows the assessed efflorescence by the proposed approach using a  $5^\circ$  threshold. The distributions of  $TP$ ,  $TN$ ,  $FP$ , and  $FN$  in Fig. 14(d) show few red pixels, but many yellow pixels in the middle and boundary of the efflorescence where the slate pencil did not apply a thick layer. In this artificial efflorescence case, the assessment was highly successful due to the purity of the calcite in the slate pencil.

### 3.5 Summary of field experiments

Table 2 shows the performance measures (i.e., accuracy, precision, and recall) of the proposed approach using  $5^\circ$  as the angle threshold for four test cases. The performance measures are obtained for both reference spectra, and the intensity thresholds that vary case by case to obtain the best assessment result in the conventional approach are tabulated together. Accuracy above 80% and precision above 70% show good performance of the proposed approach. The conventional assessment result showed relatively low recall between 57% and 77%. Because the recall values were obtained by considering the conventional assessment as “true,” the ambiguity of the conventional approach by taking a single threshold in an image may bring low recall. This is discussed in the next section.

For the reference spectra, Calcite HS48.3 outperformed Calcite CO2004 in the experiments. Calcite HS48.3 resulted in higher measures in most cases. In particular, the recall values using Calcite HS48.3B are similar or larger by up to 20% compared to those using Calcite CO2004. Thus, Calcite HS48.3B is recommended for the reference spectrum in the proposed approach. According to the fact that both reference spectra showed relatively constant results across all the experimental cases, the proposed approach detecting reference spectra is affected little by the color of the concrete surface.

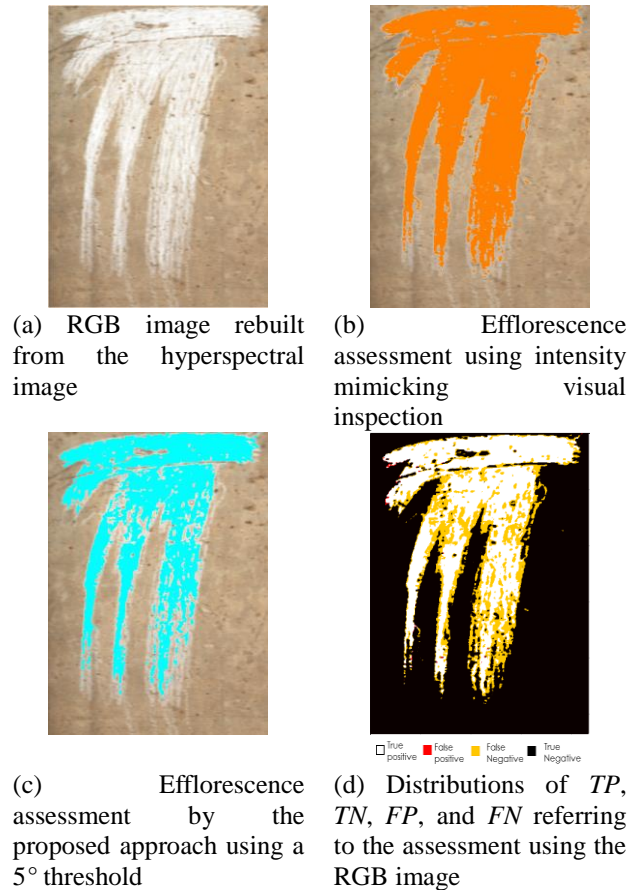


Fig. 14 Efflorescence assessment using the RGB image and by the proposed approach for P2-A

## 4. Discussion

As described in the previous section, natural and artificial efflorescence on concrete structures were assessed by the proposed approach using HSI and by the conventional approach using RGB images. As shown in Figs. 8, 10, 12, and 14, the proposed approach performs comparably to the conventional approach for W1-N, W2-N, and P2-A, and seems to outperform for P1-A with thin natural efflorescence. The results were obtained by taking single threshold values for the angle in the proposed approach and for the intensity in the conventional approach.

In this section, the three issues related to the performance of the proposed approach found during the field experiments are discussed. The issues are the validity of the angle threshold, ambiguity of the conventional approach as a reference efflorescence, and contamination of the efflorescence.

### 4.1 Validity of angle threshold for proposed approach

Because a specified value of angle threshold is not recommended for certain chemical materials, it is a critical issue to find the best threshold for the proposed approach. To propose the best threshold, performance measures by changing the angle threshold from  $2^\circ$  to  $10^\circ$  are plotted in Fig. 15 for all test cases. The reference spectrum used here

Table 2 Performance measures of the proposed approach using a 5° angle threshold

Test Cases	Reference Spectra (USGS library)	Accuracy (%)	Precision (%)	Recall (%)	Intensity thresholds for RGB images
W1-N	Calcite CO2004	90.6	98.4	64.6	90
	Calcite HS48.3B	92.6	98.2	72.6	
W2-N	Calcite CO2004	88.3	77.6	71.0	140
	Calcite HS48.3B	88.2	81.4	69.2	
P1-N	Calcite CO2004	94.1	80.2	59.0	237
	Calcite HS48.3B	92.9	81.3	74.0	
P2-A	Calcite CO2004	83.5	99.9	56.9	190
	Calcite HS48.3B	92.7	98.2	76.4	

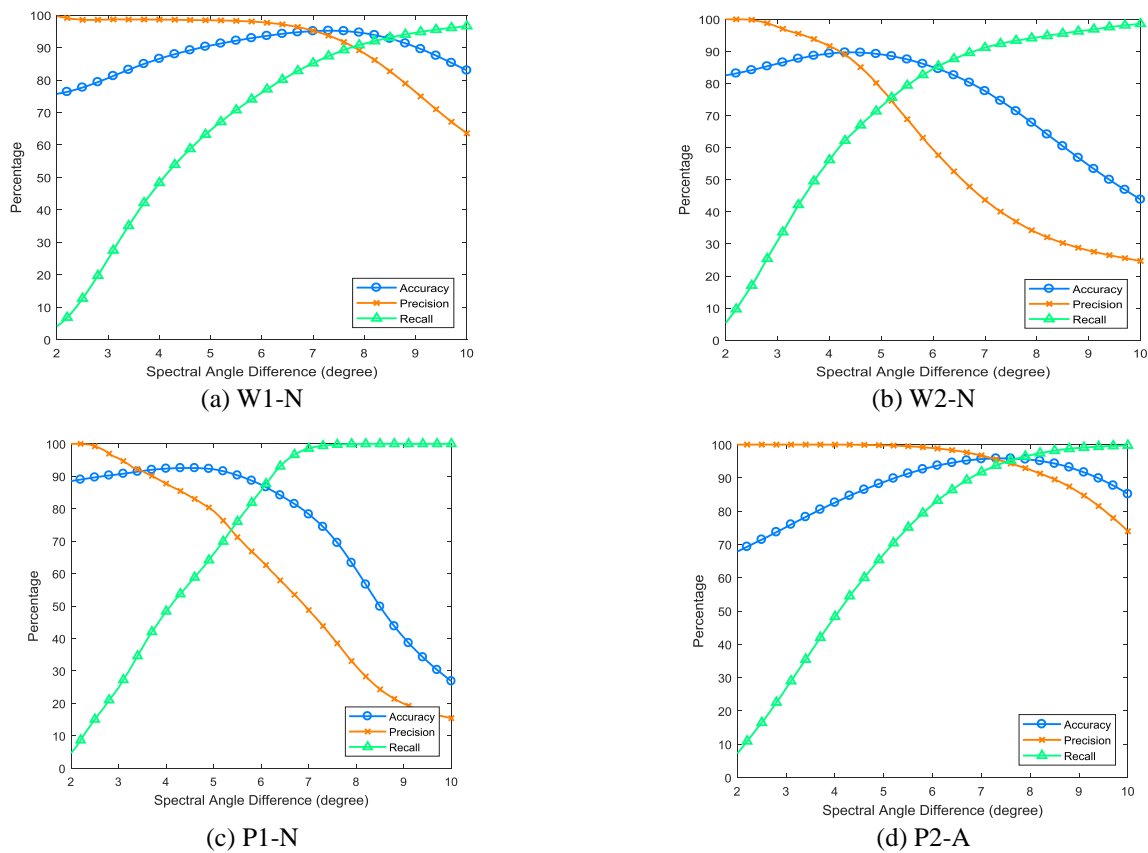


Fig. 15 Performance measures with varying threshold

is Calcite CO2004. The best accuracy is obtained at 7.5° for W1-N and P2-A, and at 5.0° for W2-N and P1-N.

This difference in best angle threshold originates from the thickness of the efflorescence; W1-N and P2-A have relatively large area of thick efflorescence, whereas W2-N and P1-N have mostly thin efflorescence. With regard to precision, high precision is observed with an angle threshold smaller than 8° in W1-N and P2-A, whereas the precision drops quickly by increasing the angle threshold in W2-N and P1-N. This implies that the proposed method accurately assesses thick efflorescence. With regard to recall related to detection of actual efflorescence, recall increases when the angle threshold increases. Recall over

85% is achieved at the 7.5° threshold for all cases. Because the result of the conventional assessment is based on a conservatively determined intensity threshold, a larger angle threshold assesses the thin efflorescence, especially near the boundary of thick efflorescence as presented in Figs. 8(b), 10(a), and 13(b). If the threshold increases, the recall is improved at the cost of sacrificing accuracy and precision.

Even though a very specific threshold value cannot be defined with the experimental cases, it is still expected that using a 5° threshold would give reliable assessment results. The ENVI software, which is widely used for hyperspectral image analysis, recommends 0.08 radian (= 4.6°) and 0.14

radian ( $= 8.0^\circ$ ) as threshold values to find “good” and “fair” matches, respectively, of a certain material based on the designated spectral library (Harris Geospatial Solutions 2017). Thus,  $5^\circ$  can be the angle threshold to find a “good” match of efflorescence, though some thin efflorescence may be missing. If thin efflorescence needs to be assessed, increasing the angle threshold up to  $8^\circ$  will provide a conservative assessment result.

#### 4.2 Ambiguity of RGB-based assessment

One of the most difficult problems in this study was to decide the “true” efflorescence in the experiment. The “true” efflorescence can be assessed by checking the chemical material composition of the efflorescence candidate using chemical analysis such as transmission electron microscope analysis. However, this chemical analysis is difficult to apply to the large area of a concrete structure. Thus, the efflorescence obtained by the conventional approach using an intensity threshold was considered as “true” efflorescence in this study. However, this consideration has ambiguity due to the single intensity threshold used for an image.

The single intensity threshold used for an image may miss thin efflorescence. In W1-N, very thin efflorescence at the upper part of the image was missed, as shown in Fig. 7. In P1-N, the start of flow near the micro crack, which is the source of efflorescence, was missed, as shown in Fig. 12. The increase of threshold can assess the missed part with exaggerated efflorescence shape. In Fig. 12, the end of flow was exaggerated even with the missing start of flow. This obscure ambiguity of “true” efflorescence influenced the evaluation of the proposed approach using performance measures.

#### 4.3 Contaminated efflorescence

Efflorescence mostly has a white color because of its major component, calcium carbonate ( $\text{CaCO}_3$ ). However, the efflorescence can be contaminated for various reasons, resulting in a change in surface color. Once contaminants are formed on efflorescence, the spectra of contaminants are mixed with that of efflorescence. Thus, the accuracy of the proposed approach using SAM is inevitably influenced by the contaminants on the efflorescence surface, because SAM calculates the spectral similarity for each pixel.

In W1-N and W2-N, brown-colored contaminants were observed on the surface of efflorescence as shown in Figs. 16(a) and 16(c). The source of the contaminants is presumed to be corrosion of rebar migrated out of the surface. The basis for this speculation is that the shape of the contaminants also forms along with the direction of water flow on the concrete surface. Obviously, the pixels corresponding to the contaminants were not labeled as efflorescence as shown in Figs. 16(b) and 16(d). With further image processing, the omitted efflorescence by the contaminants may be filled to form a solid efflorescence shape.

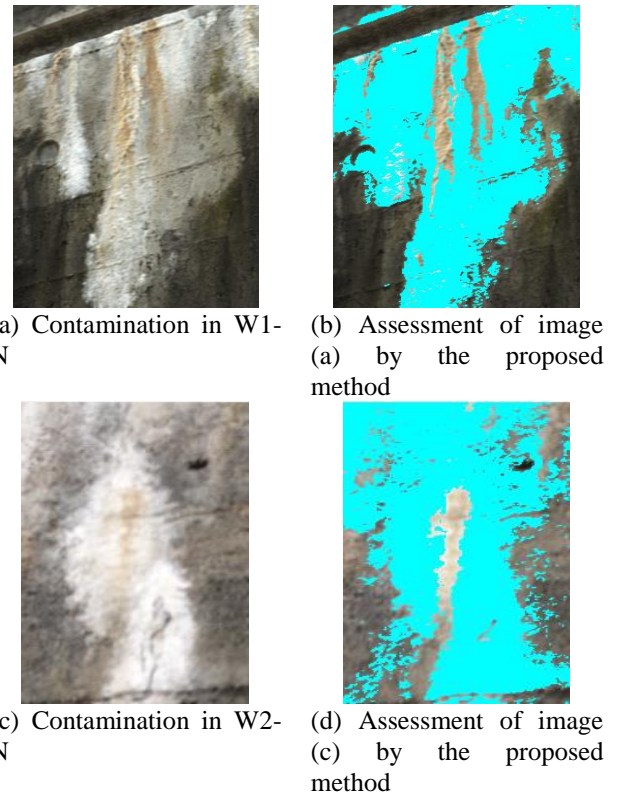


Fig. 16 Omitted efflorescence due to contamination

To enhance the assessment performance, a spectral unmixing method may be applied for contaminated efflorescence. Spectral unmixing is a widely used spectral analysis tool that decomposes a reflectance source spectrum into a set of given endmember spectra, when a pixel includes two or more different chemical components or many spectra are mixed (Bateson and Curtiss 1996).

## 5. Conclusions

In this paper, a novel approach is proposed for the objective and quantitative assessment of concrete efflorescence using HSI. Using SAM to represent the similarity of the spectral profiles as a form of angle, the proposed approach separates the pixels according to efflorescence and concrete in the image. Two reference spectra from the USGS spectral library, Calcite CO2004 and Calcite HS48.3B, were investigated for SAM. Field experiments were carried out for a concrete wall of a building and a pier of a bridge. For four types of efflorescence from the field experiments, the efflorescence distributions were obtained by the proposed approach using a  $5^\circ$  angle threshold; they were compared with those obtained by the conventional approach using RGB images. The performance of the proposed approach was measured using accuracy, precision, and recall. The results can be summarized as:

(1) In the comparison, the proposed approach could assess the efflorescence with high accuracy of over 83% and high precision of over 77% for all test cases. Recall was

found to be relatively low, between 57% and 76%, because of the ambiguity of the conventional approach that provides “true” efflorescence for comparison.

(2) Calcite HS48.3B was found to be a good reference spectrum for calculating SAM for efflorescence. In all cases, Calcite HS48.3B resulted in accuracy over 88%, precision over 81%, and recall over 69%.

(3) The proposed approach could assess thick efflorescence in W1-N and P2-A with high accuracy. Thin efflorescence distributed or at the boundary of thick efflorescence could be assessed by slightly increasing the angle threshold from 5° to 8°. The angle threshold may be adjusted according to the conservativeness of the required assessment.

(4) In the conventional approach, a single intensity threshold is used for an image. In the experiment, the thresholds varied significantly case by case because of the concrete brightness. The change in single threshold may miss thin efflorescence or exaggerate the shape of the efflorescence.

(5) Contamination of efflorescence is an obstacle for the proposed approach. A spectral unmixing method or additional image processing technique must be investigated to enhance the proposed approach.

## Acknowledgments

This research was supported by a grant (18SCIP-C116873-03) from the construction technology research program funded by the Ministry of Land, Infrastructure and Transport of the Korean government.

## References

- Adhikari, R.S., Bagchi A. and Moselhi O. (2014), “Automated condition assessment of concrete bridges with digital imaging”, *Smart Struct. Syst.*, **13**(6), 901-925.
- Arita, J., Sasaki, K.I., Endo, T. and Yasuoka, Y. (2001). “Assessment of concrete degradation with hyper-spectral remote sensing”, *Proceedings of the 22nd Asian Conference on Remote Sensing*, Singapore, November.
- BASF (2014), Efflorescence Guidelines - causes, prevention, removal, control; BASF, Ludwigshafen, Germany: [www.basf.com](http://www.basf.com)
- Baseley, D., Wunderlich, L., Phillips, G., Gross, K., Perram, G., Willison, S., Phillips, R., Magnuson, M., Lee, S.D. and Harper, W.F. (2016), “Hyperspectral analysis for standoff detection of dimethyl methylphosphonate on building materials”, *Build. Environ.*, **108**, 135-142.
- Bateson, A. and Curtiss, B. (1996), “A method for manual endmember selection and spectral unmixing”, *Remote Sens. Environ.*, **55**(3), 229-243.
- Cemex USA – Technical Bulletin (2008), Efflorescence in Concrete Products, Houston, Texas, USA: available at [http://www.cemexusa.com/ProductsServices/files/TechnicalServices/Efflorescence\\_in\\_Concrete\\_Products.pdf](http://www.cemexusa.com/ProductsServices/files/TechnicalServices/Efflorescence_in_Concrete_Products.pdf).
- Caughlin, T.T., Graves, S.J., Asner, G.P., Breugel, M., Hall, J.S., Martin, R.E. and Bohlman, S.A. (2016), “A hyperspectral image can predict tropical tree growth rates in single-species stands”, *Ecological Appl.*, **26**(8), 2367-2373.
- Chang, C.I. (2003), *Techniques for Spectral Detection and Classification*, Kluwer Academic/ Plenum Publishers, New York, USA.
- Dawood, T., Zhu, Z., and Zayed, T. (2017), “Machine vision-based model for spalling detection and quantification in subway networks”, *Autom. Constr.*, **81**, 149-160.
- Dow, C. and Glasser, F.P. (2003), “Calcium carbonate efflorescence on Portland cement and building materials”, *Cement Concrete Res.*, **33**(1), 147-154.
- ElMasry, G., Sun, D.W. and Allen, P. (2012), “Near-infrared hyperspectral imaging for predicting colour, pH and tenderness of fresh beef”, *J. Food Eng.*, **110**(1), 127-140.
- Grahn, H. and Geladi, P. (2007), *Techniques and Applications of Hyperspectral Image Analysis*. John Wiley & Sons., NJ, USA.
- Harris Geospatial Solutions (2017), Material Identification Using ENVI. Available at: <https://www.harrisgeospatial.com/docs/THORMaterialIdentification.html>.
- Jun, S., Xin, Z., Hanping, M., Xiaohong, W., Xiaodong, Z. and Hongyan, G. (2016), “Identification of pesticide residue level in lettuce based on hyperspectra and chlorophyll fluorescence spectra”, *Int. J. Agricultural Biol. Eng.*, **9**(6), 231.
- Kokaly, R.F., Clark, R.N., Swayze, G.A., Livo, K.E., Hoefen, T.M., Pearson, N.C., Wise, R.A., Benzel, W.M., Lowers, H.A., Driscoll, R.L. and Klein, A.J. (2017), USGS Spectral Library Version 7: U.S. Geological Survey Data Series 1035, 61 p.
- Kruse, F.A., Lefkoff, A.B., Boardman, J.W., Heidebrecht, K.B., Shapiro, A.T., Barloon, P.J. and Goetz, A.F.H. (1993), “The spectral image processing system (SIPS)—interactive visualization and analysis of imaging spectrometer data”, *Remote Sens. Environ.*, **44**(2-3), 145-163.
- Lee, J.D., Dewitt, B.A., Lee, S.S., Bhang, K.J. and Sim, J.B. (2012), “Analysis of concrete reflectance characteristics using spectrometer and VNIR hyperspectral camera”, *Int. Arch. Photogrammetry Remote Sens. Spatial Inform. Sci.*, **39**, B7.
- Liu, Y., Cho, S., Spencer Jr, B.F. and Fan, J. (2014), “Automated assessment of cracks on concrete surfaces using adaptive digital image processing”, *Smart Struct. Syst.*, **14**(4), 719-741.
- Man, S.H., Chang, C.C., Hassan, M. and Bermak, A. (2015), “Design and calibration of a wireless laser-based optical sensor for crack propagation monitoring”, *Smart Struct. Syst.*, **15**(6), 1543-1567.
- Ministry of Land, Infrastructure, and Transport (MOLIT) (2016), *Detailed Guidelines of Safety Inspection and Precise Safety Diagnosis for Bridges* (in Korean).
- Proto, M., Bavusi, M., Bernini, R., Bigagli, L., Bost, M., Bourquin, F., Cottineau, L.M., Cuomo, V., Vecchia, P.D., Dolce, M. and Dumoulin, J. (2010), “Transport infrastructure surveillance and monitoring by electromagnetic sensing: the ISTIMES project”, *Sensors*, **10**(12), 10620-10639.
- Santos, B.O., Valença, J., and Júlio, E. (2017), Detection of cracks on concrete surfaces by hyperspectral image processing. In *Automated Visual Inspection and Machine Vision II* (Vol. 10334, p. 1033407). *International Society for Optics and Photonics*. Munich, Germany, June.
- Taylor, H.F. (1997), *Cement Chemistry*. Thomas Telford Ltd. London, UK
- USGS Spectral Library (2017), Version 7, available at: <https://speclab.cr.usgs.gov/spectral-lib.html>.
- Vaghefi, K., Oats, R.C., Harris, D.K., Ahlborn, T.T.M., Brooks, C. N., Endsley, K.A., Roussi, C., Shuchman, R., Burns, J.W. and Dobson, R. (2011), “Evaluation of commercially available remote sensors for highway bridge condition assessment”, *J. Bridge Eng.*, **17**(6), 886-895.
- van der Werff, H.M.A. (2006), *Knowledge-based Remote Sensing of Complex Objects: Recognition of Spectral and Spatial Patterns Resulting from Natural Hydrocarbon Seepages*. Utrecht University, Utrecht, Utrecht, Netherlands

Zhang, C., Ye, H., Liu, F., He, Y., Kong, W. and Sheng, K. (2016), "Determination and visualization of pH values in anaerobic digestion of water hyacinth and rice straw mixtures using hyperspectral imaging with wavelet transform denoising and variable selection", *Sensors*, **16**(2), 244.